Synergic use of SAR imagery and high-resolution atmospheric model to estimate marine wind fields: an application in presence of an atmospheric gravity wave episode

Maria Adamo[1], Giacomo De Carolis[1], Sandra Morelli[2] and Flavio Parmiggiani[3]

[1] CNR-ISSIA, Istituto di Studi sui Sistemi Intelligenti per l'Automazione, via Amendola 122/D-I - 70126 Bari, Italia. E-mail: decarolis@ba.issia.cnr.it

[2] Dipartimento di Fisica, Università di Modena e Reggio Emilia, via Campi 213/A - 41100 Modena, Italia.

[3] CNR-ISAC, Istituto di Scienze dell'Atmosfera e del Clima, via Gobetti 101 - 40129 Bologna, Italia.

Abstract

A study aimed at retrieving sea surface wind fields of semi-enclosed basins from combined use of SAR imagery and a high resolution mesoscale numerical atmospheric model, is presented. Two consecutive ERS-2 SAR frames and a set of NOAA/AVHRR and MODIS images acquired over the North Tyrrhenian Sea on March 30, 2000 were used for the analysis. SAR wind speeds and directions at 10 m above the sea surface were retrieved using the semi-empirical backscatter models CMOD4 and CMOD-IFREMER. Surface wind vectors predicted by the meteorological ETA model were exploited as guess input to SAR wind inversion procedure. ETA is a three-dimensional, primitive equation, grid-point model currently operational at the National Centers for Environmental Prediction of the U.S. National Weather Service. The model was adapted to run with a resolution up to about 4.0 km. It was found that the inversion methodology was not able to resolve wind speed modulations due to the action of an atmospheric gravity wave, called "lee wave", which occurred in the analyzed area. A simple atmospheric wave propagation model was thus used to account for the SAR observed surface wind speed modulation. Synergy with ETA model outputs was further exploited in simulations where atmospheric parameters up-wind the atmospheric wave were provided as input to the lee wave propagation model.

Riassunto

Si descrive un esperimento per la determinazione del campo di vento sulla superficie del mare mediante l'utilizzo sinergico di immagini SAR e del modello di previsione meteorologica ETA ad alta risoluzione. L'area test selezionata è la regione del Mar Tirreno compresa tra la Corsica e le coste italiane. Per l'analisi sono state considerate due immagini ERS-2 SAR consecutive ed un set di immagini NOAA/AVHRR e MODIS del 30 Marzo 2000. Tutte le immagini evidenziano la presenza di un'onda atmosferica di gravità, che persiste per almeno 7 ore, nel tratto di mare compreso tra la penisola a N della Corsica e la costa ligure. Dall'analisi delle condizioni atmosferiche fornite da ETA, si vede che l'onda di gravità è dovuta all'ostacolo orografico che la penisola a nord della Corsica oppone al flusso d'aria proveniente da O-SO (lee wave). La velocità e la direzione del vento a 10 m dalla superficie del mare sono state ricavate dall'inversione dei modelli semiempirici CMOD4 e CMOD-IFREMER mediante un approccio di tipo Bayesiano, che utilizza l'informazione del vettore del vento fornita da ETA come dato di guess, con risoluzione orizzontale di circa 4 km. Si è riscontrato che la metodologia di inversione non è in grado di ricostruire le modulazioni della velocità del

vento dovute alla manifestazione dell'onda di gravità. Per tener conto della modulazione della velocità del vento è stato considerato un semplice modello di propagazione di lee waves che tiene conto delle caratteristiche geometriche dell'ostacolo e della struttura verticale dell'atmosfera ad esso antistante. Si dimostra che l'uso dei profili verticali dei parametri atmosferici predetti dal modello ETA, in input al modello di lee waves, è in grado di riprodurre la modulazione della velocità del vento, osservata sull'immagine SAR, entro i limiti di accuratezza dei modelli CMOD considerati.

Introduction

In the last few years scientific efforts of the remote sensing community are being focused on the study of procedures able to retrieve geophysical parameters from satellite data. In particular, the unique capability of Synthetic Aperture Radar (SAR) imagery to provide high resolution (1-10 km) wind fields in the marine environment is being pursued. As the wind field has two components, namely speed and direction, the inversion of the single SAR normalized radar cross section (NRCS) is however an undetermined problem. To solve it, two classes of SAR inversion procedures have been envisaged, both relying upon external wind information. Regarding to the available inversion procedures for C-band operating SAR systems, the geophysical relationship between the observed NRCS and the corresponding wind vector is provided by semi-empirical backscatter models belonging to the C-band MODels (CMOD) family [Stoffelen and Anderson, 1997; Quilfen et al., 1998]. Originally developed on a statistical basis to associate the NRCS measured by the ERS scatterometers to the wind vector blowing over the imaged area, these backscatter models were later successfully exploited on ERS SAR imagery [Lehner et al., 1998]. The first class of inversion procedures is based on the a priori knowledge of the wind direction, usually gathered by anemometers located within the region of interest or estimated directly on the SAR image by means of the recognition of wind rows [Wackerman et al., 1996; Fetterer et al., 1998; De Carolis et al., 2004]. Given the wind direction, the wind speed is retrieved as the optimal value which minimize the difference between the observed NRCS and the simulated one. The second class is instead based on the exploitation of mesoscale atmospheric model outputs [Portabella et al., 2002]. Here the forecasted wind vector is used as guess to initialize the inversion procedure. While the measured wind vector is usually limited to a few instrumented sites scattered within the region of interest, wind fields predicted by mesoscale atmospheric models are able to capture the main features of the atmospheric flow over a regular grid whose size settles the spatial resolution of the SAR retrieved wind field. In contrast, mesoscale models may fail in predicting peculiar atmospheric processes of the lower atmospheric boundary layer, which superimpose to the main air flow and give rise to an additional NRCS modulation at spatial scales often comparable to that of the SAR wind inversion procedure. A remarkable example is represented by the internal atmospheric gravity waves, called "lee waves". Commonly occurring both over land and sea surface in the lee side of terrain barriers, they are supported either by stably stratified lower troposphere or by vertical wind shears upstream the barrier [Gossard and Hooke, 1975]. The dominant wave length usually ranges from less than 1 km to few tens of km and may extend over several wave lengths downstream the barrier [Thomson et al., 1992; Vachon et al., 1994; Alpers and Stilke, 1996]. In presence of stationary airflow, stationary atmospheric waves may develop, thereby lasting for several hours and causing the formation of spectacular cloud bands aligned with the wave vector and nearly perpendicular with the surface wind blowing upstream the barrier. Visible and thermal satellite imagery can document such cloud bands both over land and ocean [Thomson et al., 1977; Gjevik and Marthinsen,

1978; Gjevik, 1980]. Over the sea surface, atmospheric waves modulate the horizontal wind speed blowing downstream the barrier, thus allowing their detection as periodic SAR NRCS modulation [Vachon et al., 1994; Alpers and Stilke, 1996; Chunchuzov et al., 2000]. The formation and evolution of atmospheric gravity waves are mainly determined by the vertical structure of the atmospheric boundary layer upstream the disturbing topographic barrier. So far, radiosonde data were extensively used to study the spatial arrangement of lee waves, as demonstrated for the first time by Gjevik and Marthinsen [1978]. However, it may only rarely happen that available radiosonde data are co-located both in space and time to a manifestation of atmospheric gravity wave train. In contrast, an accurate atmospheric model could provide the required atmospheric data at the desired space-time location to study the physical characteristics of the wave phenomenon.

In this paper predictions from the numerical mesoscale atmospheric model ETA at high horizontal and vertical spatial resolutions are considered for twofold applications: 1) to drive a SAR surface wind inversion procedure over a selected area in the Northern Tyrrhenian Sea, which includes eastern Lygurian Sea and the northern Corsica Island; 2) to assess SAR observation of an internal atmospheric wave visible in the same area by using the ETA predicted vertical profiles of atmospheric parameters. As horizontal and vertical structures predicted by ETA show little evidence of atmospheric wave pattern at the used resolutions, a specialized lee wave model is considered to validate SAR observations of wind modulation. The atmospheric wave pattern has also been compared with complementary MODIS and NOAA/AVHRR imagery in order to improve SAR image interpretation and to substantiate lee wave model feasibility with respect to the observed wave lengths.

ETA model description

The ETA atmospheric model is a three-dimensional, primitive-equation, grid-point model. It uses a rotated spherical coordinate system, and a semi-staggered Arakawa E grid. The vertical coordinate is the so-called η coordinate, which represents a generalization of the usual σ coordinate. The η coordinate is defined as [Mesinger, 1984]:

$$\eta = \frac{p - p_t}{p_s - p_t}\eta_s \qquad [1]$$

where $\eta_s = (p_{rf}(z_s) - p_t) / (p_{rf}(0) - p_t)$. Here p_t and p_s are the model top and the surface pressure, respectively, z is the geometric height and $p_{rf}(z)$ is a suitably defined reference pressure as a function of z. The η-coordinate surfaces are almost horizontal. However the model can perform run with terrain following coordinates as well. The so-called "silhouette mountains" are constructed from the Digital Elevation Model (DEM) dataset at 30" by 30" horizontal resolution. The model topography, obtained by rounding off the silhouette values, is represented by step-mountains: the ground surface heights, z_s are allowed to take only discrete values, chosen so that mountains are constructed from three-dimensional grid boxes. The velocity components at the sides of mountains are set to zero. The vertical layers of the model atmosphere are thin near sea level, thickening as one goes higher. Prognostic variables are temperature, specific humidity, horizontal components of velocity, surface pressure, cloud water and turbulent kinetic energy. Sea surface temperature (SST), interpolated to the ETA model grid, is held constant at the initial value. The model is able to perform hydrostatic or non-hydrostatic runs. Physical parameterizations (including references for the various parameterizations) are presented in Cesini et al. [2004]. A version of ETA model is currently operational at the National Centers for Environmental Prediction (NCEP) of the U.S. National Weather Services.

The model simulations, presented in this paper, are carried on with three nested domains

in order to obtain the high horizontal resolution. The technique used is a one-way nesting. The European Centre for Medium Range Weather Forecasts (ECMWF) initialized analyses, at 0.5° x 0.5° horizontal resolution, provided initial and boundary conditions for the lower resolution ETA model run. Initial conditions refer to 00:00 UTC 29 March 2000 and the simulations last 72 hours. Model outputs of the first domain are used as boundary conditions of the second grid run and this provides the boundary conditions for the finer grid run. Vertical resolution consists of 50 layers from sea surface to 25 hPa, with higher resolution near the bottom of the domain. Horizontal resolution is 0.125 x 0.125 transformed degrees (about 20 km x 20 km as approximate distance between two mass points on the semi-staggered Arakawa E grid) for the coarse grid, 0.05 x 0.05 transformed degrees (about 7.5 x 7.5 km^2) for the second grid and 0.025 x 0.025 transformed degrees (about 4 x 4 km^2) for the finer grid [Morelli and Berni, 2003; Cesini et al., 2004]. The domain size of the coarse resolution run is 19° x 20° transformed degrees with central point located at 43.5°N, 9.5°E. Time step is 36 seconds; the boundary conditions are updated every 6 hours. The second grid simulation is performed with a domain size of 8° x 8° transformed degrees. Time step is 15 seconds; the boundary conditions are updated every 3 hours. The finer grid non-hydrostatic run uses a domain of 4° x 4° transformed degrees. Time step is 10 seconds, updating the boundary conditions every hour. Model outputs for the finer grid are extracted every hour.

Atmospheric gravity waves: model description

When air flow impinges upon a terrain obstacle, the disturbance causes displacement of the air from equilibrium position in the lee side of the obstacle. As a result, air parcels start to oscillate generating internal atmospheric waves restored by gravity.

These waves, also called “lee waves” or “mountain waves”, are usually supported by stably stratified layers in the lower troposphere, which act as waveguide [Gossard and Hooke, 1975]. The occurrence of atmospheric waves is often associated with the formation of periodic cloud bands whose orientation is nearly perpendicular to the surface wind direction [Worthington, 2001]. If lee waves propagate over the ocean surface, the corresponding wind speed variation modulates the local surface roughness, which in turn is detected as NRCS modulation on SAR images.

Purpose of this section is to review the simple lee wave model developed by Palm and Foldvik [1959] which predicts the expected surface wind modulation. Air flow downstream the terrain barrier is modeled on the following assumptions: 1) the barrier is infinitely long and approximated by a bell-shaped function; 2) the wind blows parallel to the short side of the barrier. For the case studies herein presented, both conditions are only approximately fulfilled. The terrain barrier is represented by the peninsula north of Corsica, which is approximately stretched out into N-S direction with width/length ratio of about 1:3; besides, ETA provided a height-averaged wind speed components ratio $V/U \cong 0.32$. We thus expected that the lee wave model predictions can only partially support satellite observations.

In the reference bi-dimensional Cartesian space x-z, where x is the downstream direction and z is the vertical direction pointing upwards from the ground placed at $z = 0$, the two-dimensional air parcel oscillations can be described by the Scorer parameter $l = l(z)$ defined as follows [Palm and Foldvik, 1959]:

$$l^2 = \frac{S}{U^2} - \frac{1}{U}\frac{d^2U}{dz^2}, \qquad [2]$$

where $S = g\,(d\theta/dz)\,/\,\theta$ is the atmospheric stability parameter; $U = U(z)$, $\theta(z)$ are the horizontal wind speed and the potential temperature upstream the barrier; g is the acceleration due to gravity. The Scorer parameter in the lower atmosphere up to about 10 km can be usually

represented by the exponential function $l(z) = l(0)\exp(-cz)$, even if abrupt changes of l due to thin inversion layers may occur.
As a result, the wave-like solution of the horizontal velocity u modulating the upstream wind speed U can be written as [Palm and Foldvik, 1959; Foldvik, 1962]:

$$u_B(x,z) = 2\pi HU(0)be^{\beta z/2} \cdot$$

$$\sum_{k=k_r} e^{-kb} \frac{\left(\frac{1}{2}\beta - \frac{1}{U(z)}\frac{\partial U}{\partial z}\right) J_{k/c}\left(l(z)/c\right) - l(z)\frac{\partial}{\partial\left(l(z)/c\right)} J_{k/c}\left(l(z)/c\right)}{\frac{\partial}{\partial k} J_{k/c}\left(l(0)/c\right)} \sin kx, \quad x > 0 \qquad [3]$$

where β is the exponent of the adiabatic atmosphere $\rho(z) = \rho(0)\exp(-\beta z)$. The above expression holds for a bell-shaped ridge $\zeta_B(x,0) = Hb^2/(b^2+x^2)$, where H is its height and b the half-width. The sum in [3] is performed on the resonant wavenumbers forming the lee wave pattern obtained as solution of the equation:

$$J_{k/c}\left(\frac{l(0)}{c}\right) = 0, \qquad [4]$$

where J denotes the Bessel function of the first kind.
For the sake of comparison with the available SAR image, we found that the barrier relevant to our case study (Corsica peninsula) could also be represented by a Gaussian-shaped function $\zeta_G(x,0) = H\exp(-a^2x^2)$. The corresponding modulating horizontal velocity $u_G(x,z)$ has the following expression:

$$u_G(x,z) = 2\sqrt{\pi}\frac{H}{a}U(0)e^{\beta z/2} \cdot$$

$$\sum_{k=k_r} e^{-(k/2a)^2} \frac{\left(\frac{1}{2}\beta - \frac{1}{U(z)}\frac{\partial U}{\partial z}\right) J_{k/c}\left(l(z)/c\right) - l(z)\frac{\partial}{\partial\left(l(z)/c\right)} J_{k/c}\left(l(z)/c\right)}{\frac{\partial}{\partial k} J_{k/c}\left(l(0)/c\right)} \sin kx, \quad x > 0 \,. \qquad [5]$$

SAR wind inversion procedure

Wind speed at 10 m above the mean sea level can be estimated from SAR imagery using semi-empirical models developed from the C band, VV polarised ERS-1/2 scatterometer measurements. Backscatter predictions of the CMOD4 [Stoffelen and Anderson, 1997] and CMOD-IFREMER [Quilfen et al., 1998] empirical models were herein considered for SAR inversion procedure. They are based on the following functional dependence:

$$\sigma_0 = b_0(W,\theta)[1+b_1(W,\theta)\cos(\phi) + b_2(W,\theta)\cos(2\phi)]^n \qquad [6]$$

where σ_0 is the SAR backscatter value, (W, ϕ) are the neutral 10 m wind speed and direction and θ is the incidence angle of the radar beam. The exponent n has a value 1.6 for CMOD4 and 1 for CMOD-IFREMER model. Parameters b_i's were statistically determined after comparison with wind data from the ECMWF atmospheric model outputs for CMOD4 model and from operational buoy measurements for CMOD-IFREMER model.
The inversion of [6] can be accomplished only if perfect *a priori* knowledge of one of the two geophysical wind components is available. In alternative, starting from a general statistical approach used in meteorological analysis to solve inversion problems [Lorenc,

1986], [Portabella et al., 2002] proposed the minimization of the cost function [7] to obtain the most probable wind vector from the combined use of SAR backscatter and background information provided by a numerical atmospheric model. We adopted the latter approach. Wind vectors predicted by the ETA model over wind cells with 4 x 4 km^2 horizontal resolution were made available to us in order to assess the ETA model potential to base its predictions for studying complex atmospheric phenomena such as internal gravity waves propagating in the atmosphere. To accomplish the task, SAR imagery was calibrated and then the averaged backscatter over the corresponding ETA wind cell was considered to retrieve the most probable wind vector. The cost function has the following expression:

$$J = \left(\frac{\sigma^o_{SAR} - \sigma^o_{MODEL}}{\Delta\sigma^o_{SAR}} \right)^2 + \left(\frac{U_{ETA} - U_{TRIAL}}{\Delta U_{ETA}} \right)^2 + \left(\frac{V_{ETA} - V_{TRIAL}}{\Delta V_{ETA}} \right)^2 \qquad [7]$$

where σ^0_{SAR} is the averaged SAR NRCS corresponding to the co-located ETA wind cell and σ^0_{MODEL} is the simulated NRCS using the C band model functions with the trial wind vector (U_{TRIAL}, V_{TRIAL}). For a particular wind cell, the trial wind components U_{TRIAL} and V_{TRIAL} were allowed to vary over a wide range of values with step size of 0.1 ms^{-1} around the corresponding ETA wind components U_{ETA} and V_{ETA}. It was assumed that the uncertainty associated to the ETA wind vector (U_{ETA},V_{ETA}) was ΔU_{ETA}=ΔV_{ETA} = 1.73 ms^{-1} at the used horizontal resolution [Portabella et al., 2002]. The error $\Delta\sigma^0_{SAR}$ represents the average NRCS variability and was found to obey the following relationship for the set of ERS images herein considered: $\Delta\sigma^0_{SAR}$ = 0.0754xσ^0_{SAR} .The wind vector (U_{TRIAL}, V_{TRIAL}) that minimizes J was retained as the best wind vector estimation for a particular wind cell.
Wind maps retrieved from the ERS SAR images used in this study will be discussed in the next section.

The experiment

A pair of ERS-2 SAR Precision Images of the Northern Tyrrhenian Sea acquired on March 30, 2000 at 10:08 UTC (orbit: 25842, frames: 2727, 2745) and relevant to an area that extends from 42.2 N to 44.0 N and 8.8 E to 10.5 E was considered. Geographical boundaries include the northern peninsula of Corsica and the eastern part of the Lygurian coast.
The western edge of the Elba Island is also imaged. On 10:40 UTC the Moderate Resolution Imaging Spectroradiometer (MODIS) on board the EOS Terra satellite acquired an image including the SAR imaged area at 250 m resolution. Both SAR and MODIS images are shown in Figure 1. Visual inspection of SAR images reveals that sea surface NRCS is modulated by a periodic pattern approximately aligned with the 10 m wind vector blowing from W-SW, as predicted by ETA model. The pattern can be interpreted as sea surface manifestation of atmospheric wind rolls, which form in the planetary boundary layer as a consequence of the helicoid motion of the air flow [Alpers and Brummer, 1994].
MODIS image shows a clear periodic cloud band pattern that extends eastward from the Corsica peninsula, crosses the expanse of sea north of Elba Island and continues over the Italian inland. Co-located with the cloud pattern, a similar NRCS pattern can be seen on SAR image. Figure 1 shows SAR and MODIS insets of the common area along with the averaged azimuth profile. The periodic SAR backscatter modulation can be associated to a convective motion of air parcels generating the cloud band pattern to which corresponds a periodic, horizontal surface air flow [Thomson et al., 1992; Vachon et al., 1994]. Later in the paper it will be shown that cloud pattern is originated by the propagation of an internal atmospheric wave resulting from the westerly air flow coming up against the Corsica peninsula.

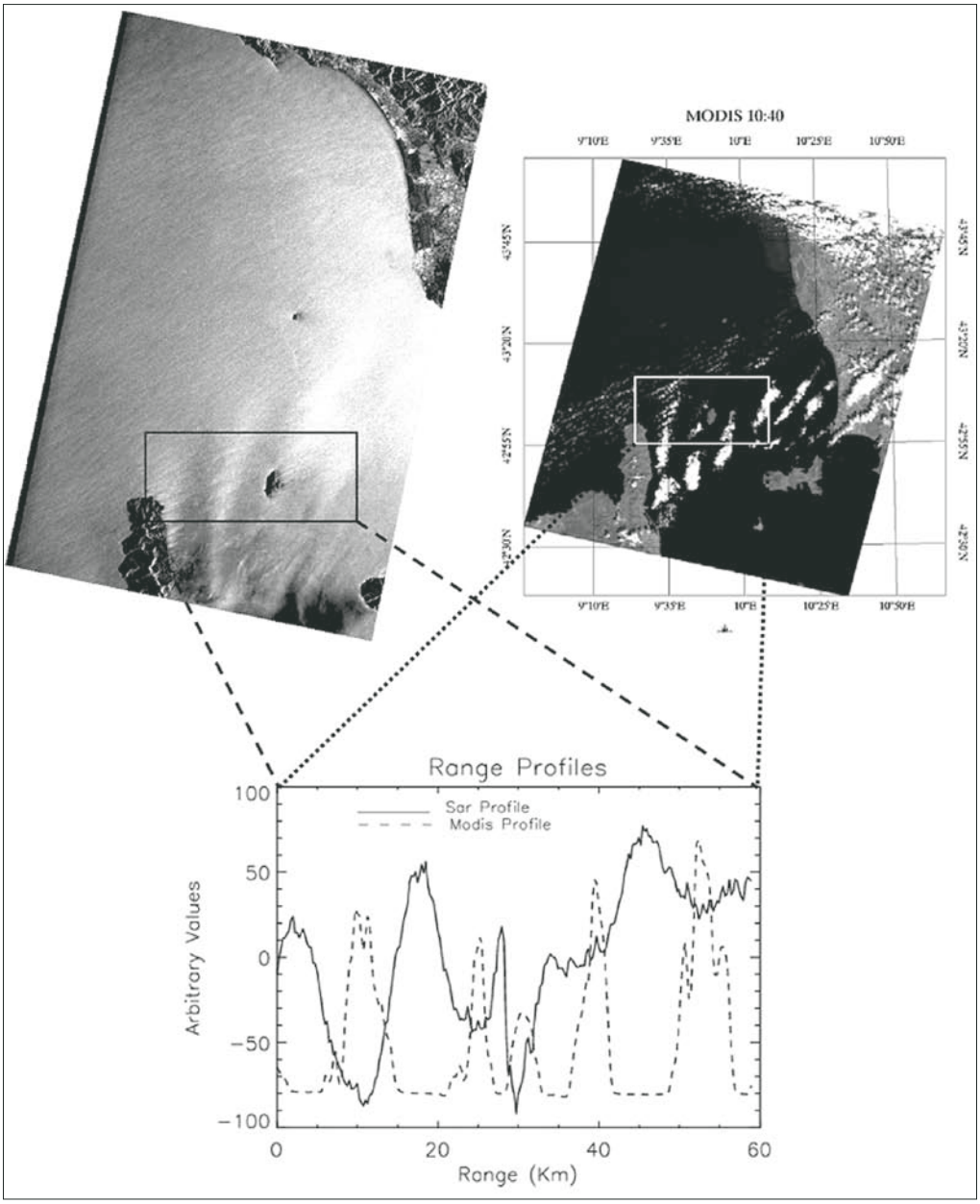

Figure 1 - Composite of ERS-2 SAR images (left) and MODIS image (right) acquired on March 30, 2000 at 10:08 and 10:40 UTC, respectively. Insets show periodic modulation of SAR NRCS and a corresponding cloud band on MODIS image, both originating from the occurrence of an atmospheric gravity wave. The bottom plot shows averaged SAR and MODIS lines. The cloud pattern is out of phase with NRCS modulation.

Figure 2 shows a synoptic view of the SAR retrieved wind speed and direction for each cell using CMOD4 with superimposed the corresponding ETA predictions; besides, scatter diagrams of Figure 3 report the horizontal components (U,V) of the retrieved wind vector

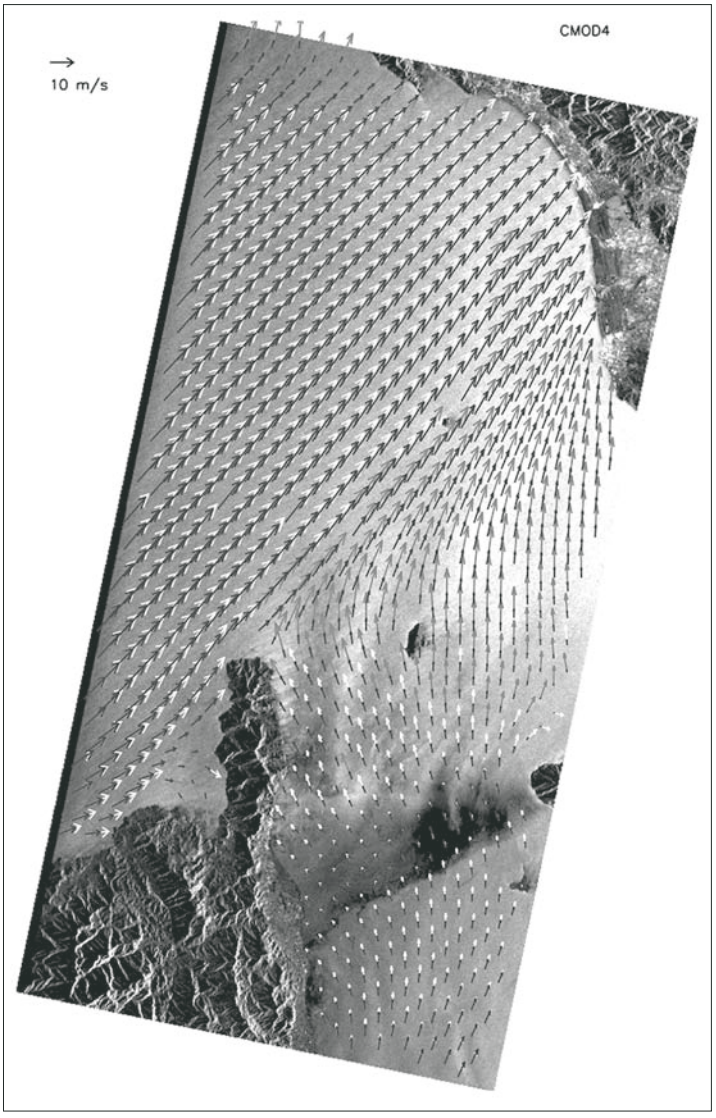

Figure 2 - Retrieved wind map after SAR inversion with CMOD4 semi-empirical backscatter model. Spatial resolution of SAR wind cells is about 4 km. ETA wind field is drawn with black arrows. White arrows represent retrieved wind vectors with low value (<10) of residual cost function *J*; grey arrows represent retrieved wind vectors relevant to wind cells with high value (>10) of residual cost function *J*.

(panels 1 and 2), wind speed (panel 3) and wind direction (panel 4) vs the corresponding ETA components for quantitative comparison. As similar inversion results were obtained using CMOD-IFREMER, we will refer hereafter to CMOD4 only.

In general, the SAR inversion procedure corrected ETA wind speeds toward higher values. Specifically, an overall bias of about +5 ms^{-1} resulted for wind cells whose residual value of the cost function was J >10 (grey arrows in Figure 2 and black points in the panels of Figure 3). They mainly correspond to SAR imaged areas located on the lee side of Corsica peninsula, where an atmospheric gravity wave is active, and, as expected, to areas close to the Ligurian coast [Lehner et al., 1998]. For wind cells with residual J<10 (white arrows in Figure 2 and gray points in panels of Figure 3), the retrieved SAR wind speeds resulted in average about 1.5-2.0 ms^{-1} higher than ETA wind speeds. Assuming ETA wind vec-

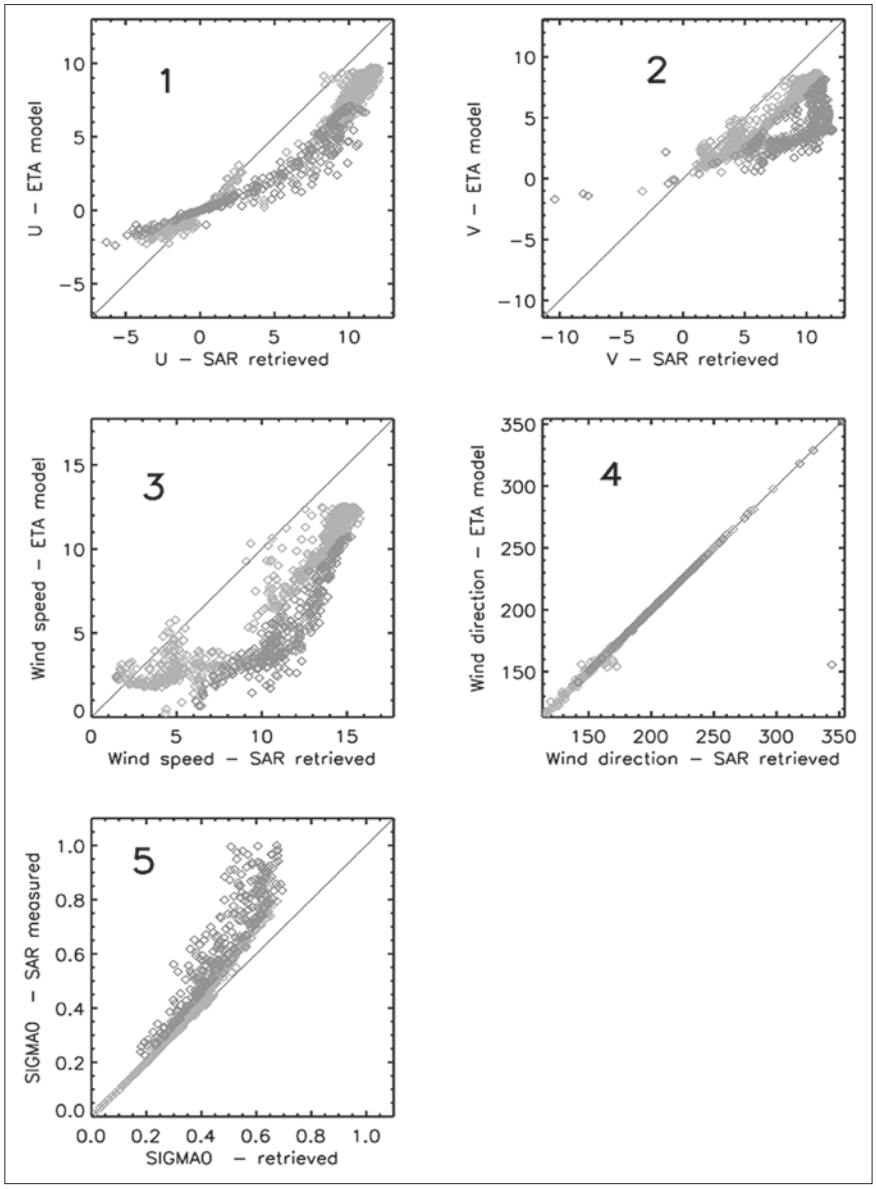

Figure 3 - Scatter diagrams representing the performances of the SAR inversion procedure using CMOD4 model.

tors reasonably representative of the real wind vector, the corrective bias compares with the expected average rms uncertainty assigned to CMODs performances [Wackerman et al., 1996; Fetterer et al., 1998]. In contrast, the retrieved wind directions resulted not significantly different to ETA directions, regardless the residual *J* value. This result may be twofold interpreted: 1) the main contribution of CMOD4 is relevant to wind speed since wind directions predicted by ETA model are within the CMOD4 direction accuracy of ±20°, according to the geophysical specification of the ERS-1/2 scatterometers [Vass and Battrick, 1992]; or 2) the SAR inversion procedure is not able to correct the input wind di-

rection, although the retrieved U and V components are individually modified. Although this aspect of the SAR inversion procedure deserves further investigation, for the purpose of the present paper it can be concluded that SAR detected complex atmospheric phenomena, such as atmospheric gravity waves, that superimpose to the main air flow predicted by mesoscale atmospheric modeling, should be properly handled. Another aspect of the SAR inversion procedure performance is the introduction of slight biases in the predicted CMOD4 NRCS, as drawn in the panel 5 of Figure 3. It can be seen that for wind cells with $J < 10$ (grey points in Figure 3), the average NRCS bias between SAR and CMOD4 is about 0.32 ± 0.19 dB for $\sigma^0_{SAR} \geq 0.45$ (~ -3.45 dB), *i.e.* for wind speeds not lower than about 11 ms^{-1}; the bias increases to 1.19 ± 0.51 dB for wind cells with residual cost function $J > 10$. The backscatter bias can be readily explained by considering that the couple (U,V) for which J assumes the minimum value does not necessarily minimize each term of the cost function. So, the backscatter bias is not surprising: the closer are the ETA wind components predictions to the true values, the lower the backscatter bias will result.

Figure 4 shows the temporal sequence of four near-infrared/visible images relevant to the area under study gathered on March 30, 2000 since 03:17 UTC. They include the evolution of a periodic cloud pattern associated to a stationary atmospheric lee wave. The last image was acquired by MODIS at 10:40. Images gathered before 03:17 and after 10:40 do not

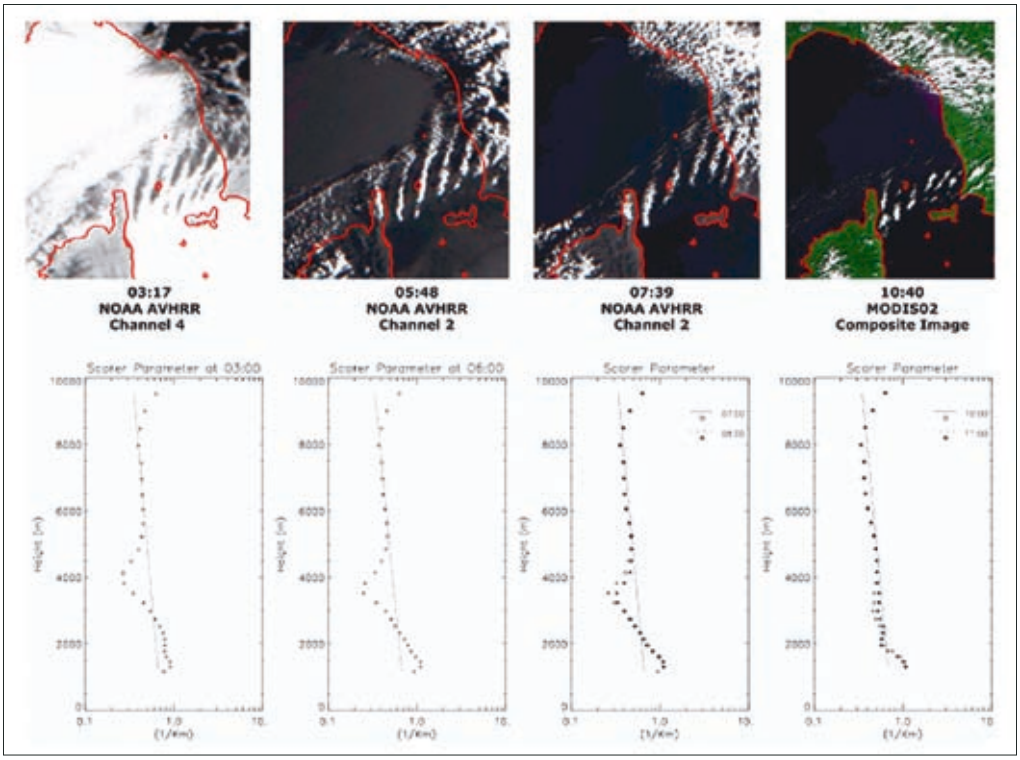

Figure 4 - Temporal sequence of satellite images showing evolution of the cloud band generated by quasi-stationary atmospheric lee wave. The lower panel shows the Scorer profile computed using ETA atmospheric parameters up-stream the terrain barrier (peninsula of Corsica) extracted at minute 00 of the closest hour to image acquisition. For NOAA/AVHRR acquisition at 07:39 and MODIS acquisition at 10:40, the Scorer parameters at minutes 00 of the hours before and after image acquisition are shown. The exponential fit is superimposed for each Scorer profile.